THE JOURNAL OF PHYSICAL CHEMISTRY B

Article

Cite This: J. Phys. Chem. B 2018, 122, 5897−5907

pubs.acs.org/JPCB

Influence of Cholesterol on the Dynamics of Hydration in Phospholipid Bilayers

M. Dolores Elola*,† and Javier Rodriguez†,‡

†Departamento de Física, Comisión Nacional de Energía Atómica, Av Libertador 8250, 1429 Buenos Aires, Argentina

‡ECyT, UNSAM, Martín de Irigoyen 3100, 1650 San Martín, Provincia de Buenos Aires, Argentina

Supporting Information

ABSTRACT: We investigate the dynamics of interfacial waters in dipalmitoylphosphatidylcholine (DPPC) bilayers upon the addition of cholesterol, by molecular dynamics simulations. Our data reveal that the inclusion of cholesterol modifies the membrane aqueous interfacial dynamics: waters diffuse faster, their rotational decay time is shorter, and the DPPC/water hydrogen bond dynamics relaxes faster than in the pure DPPC membrane. The observed acceleration of the translational water dynamics agrees with recent experimental results, in which, by means of NMR techniques, an increment of the surface water diffusivity is measured upon the addition of cholesterol. A microscopic analysis of the lipid/water hydrogen bond network at the interfacial region suggests that the mechanism underlying the observed water mobility enhancement is given by the rupture of a fraction of interlipid water bridge hydrogen bonds connecting two different DPPC molecules, concomitant to the formation of new lipid/solvent bonds, whose dynamics is faster than that of the former. The consideration of a simple two-state model for the decay of the hydrogen bond correlation function yielded excellent results, obtaining two well-separated characteristic time scales: a slow one (∼250 ps) associated with bonds linking two DPPC molecules, and a fast one (∼15 ps), related to DPPC/solvent bonds.

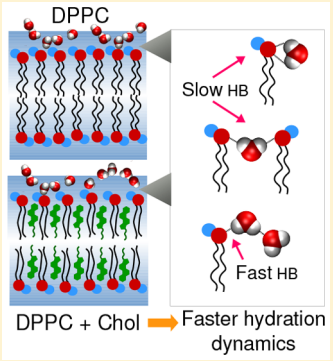

1. INTRODUCTION

Phospholipid bilayers represent fundamental structures of a great variety of biomembranes. Lipid membranes are known to govern various biologically relevant processes at the cellular level. Hydration water in the vicinity of these biomolecular surfaces plays a crucial role within these scenarios, modulating the structural organization of the constituents and their functions. The characteristics of membranes have been extensively studied in past decades; experiments have provided valuable information about physical chemistry properties of membrane systems.[1−4] However, it is often difficult to attain a complete understanding of the phenomena taking place in lipid membranes exclusively from experimental measurements. In this sense, atomistic computer simulation studies provide a complementary and powerful tool for a thorough comprehension of these systems at the microscopic level.[5−10]

In this work, we employed atomistic molecular dynamics (MD) simulations to investigate fully hydrated lipid bilayers composed of pure dipalmitoylphosphatidylcholine (DPPC) and mixtures of DPPC with cholesterol (Chol). Cholesterol is one of the most important steroid species in nature; it can be found in high concentrations in animal cell membranes in typical concentrations of 20−30 mol %, and up to 50 mol % in red blood cells. The effects of cholesterol on cell membranes and functions range from mechanic to metabolic ones. Among the former, the ordering and condensing properties[11−13] are well-known effects of cholesterol embedded in lipid membranes. The ordering effect has been measured by various experimental techniques, including NMR, EPR, and fluorescence spectroscopy,[12,14,15] and has also been reproduced by computer simulations.[4,7,16,17] The condensing effect is defined as the decrease of the area per lipid upon addition of cholesterol. Both effects, ordering and condensing, are closely related and have been extensively reported in the literature.[4,18−21]

Our work was inspired by interesting experimental results recently obtained by Cheng and collaborators,[22] focused on the dynamical role of hydration waters in Chol-embedding lipid membranes, by Overhauser dynamic nuclear polarization (ODNP) NMR relaxometry techniques. On the basis of measurements of the translational correlation time of water, the authors report an increment in the surface water diffusivity, along with a much slower mobility within the bilayer interior, at high Chol concentrations. The results suggest that local hydration dynamics is altered over a region of 5−10 Å around the lipid head group surface, exhibiting a faster water diffusivity compared to Chol-depleted DPPC surfaces. Moreover, their data also show that the addition of Chol to the lipid membrane produces a decrease in the order and packing of the lipid head groups. These experimental findings, i.e., the enhancement of the surface water dynamics and decreased order of the lipid head groups induced by cholesterol, had never been either reported experimentally or predicted theoretically by prior studies. Therefore, we consider that a computational approach

Received: January 11, 2018
Revised: May 7, 2018
Published: May 9, 2018

DOI: 10.1021/acs.jpcb.8b00360
J. Phys. Chem. B 2018, 122, 5897−5907

to the microscopic analysis of these systems can clearly contribute to a better understanding of these phenomena.

The paper is organized as follows: in Section 2 we describe the systems studied and the potential models, along with simulations details. In Section 3 we present and discuss the results obtained for the structural and dynamical properties. We conclude in Section 4 with a summary of our main findings.

2. COMPUTATIONAL DETAILS

To investigate the dynamics of water in contact with a lipid membrane containing cholesterol, we have simulated a lipid bilayer system consisting of 968 lipid molecules (i.e., 484 lipids in each leaflet), surrounded by 30 600 water molecules. These numbers correspond to ∼32 waters per lipid and represent a fully hydrated state of the bilayer.[23] The overall potential energy of the system was considered as a sum of site−site, pairwise interactions combining Lennard-Jones and Coulomb contributions. For DPPC and cholesterol species, we adopted a previously validated united-atom model[17] for the nonpolar CH_2/CH_3 groups in the ammonium head group of DPPC and hydrocarbon tails, reducing the number of atoms per DPPC molecule down to 50, and 29 for cholesterol. Atomic charges for the DPPC molecules were taken from ab initio calculations.[24] The electronic charges of the cholesterol head were distributed with +0.40*e* on the hydrogen, −0.54*e* on the oxygen, and +0.14*e* on the carbon to which the hydroxyl group is attached.[17]

Starting with a fully hydrated DPPC bilayer, we performed a preliminary equilibration run for 10 ns at T = 323 K. To generate the DPPC/Chol systems with cholesterol mole fractions of x_{chol} = 0.30 and 0.50, a given number of DPPC molecules were randomly chosen (same quantity on each leaflet) and replaced by cholesterol, orienting the polar head group toward the aqueous phase. In addition, successive equilibration runs were performed, in which either the head group sites or the hydrophobic tails were alternatively thermalized at 350 K. Following this initial accommodation of the DPPC and Chol molecules in the bilayer, we run a 10 ns trajectory at T = 323 K for the fully hydrated systems. During this period, the area ($A_{BOX} = L_x \times L_y$, $L_x \equiv L_y$) and length of the simulation box along the z-axis (L_z) were adjusted to set the pressure to P = 1 atm and to tune the aqueous local density away from the bilayer to the water bulk value. All molecular dynamics (MD) trajectories were generated using the NAMD package[25] and corresponded to NVT canonical runs. The particle mesh Ewald (PME) method was implemented to handle long-range Coulomb forces.[26] The equations of motion were integrated using a multiple time step scheme, with a time step of 2 fs for intramolecular modes and nonbonded short-range forces, and 4 fs for the rest of the Coulomb forces.

Figure 1 shows a typical snapshot of the equilibrated system and a scheme of DPPC and cholesterol molecules, whereas Table 1 depicts the details of some relevant parameters used for the simulations. Two key features are worth remarking: (i) the area per lipid (APL) obtained in the pure DPPC membrane, 0.645 nm^2, is in good agreement with previous simulation results[27−29] and experimental data;[2,23] and (ii) there is a 30% reduction in the area of the simulation box, observed in going from the pure DPPC membrane to one with x_{chol} = 0.50 (APL = 0.454 nm^2), while keeping the total number of lipids (DPPC + Chol) constant. Falck et al.[30] and Issack and Peslherbe[10] have also studied DPPC/Chol systems by computer simulations in a similar Chol concentration range as in the present work. Falck et al. report APL values of 0.64, 0.42, and 0.38 nm^2 for x_{chol} = 0, 0.30, 0.50, respectively, but using a different force field and performing their MD simulations under an NpT ensemble. Employing a slightly different version of the force field used by Falck et al., Issack and Peslherbe[10] obtained APL values of 0.62, 0.48, and 0.41 nm^2 for the same series of Chol concentrations. Although the agreement between our predicted APL and those from the studies of Falck and Issack is very good for the cholesterol-free DPPC system, the comparison yields a lower overlap among the computed APL values in the DPPC/Chol membrane systems. More precisely, our estimation for the APL in DPPC/Chol membranes predicts a reduction of 30% when going from x_{chol} = 0 to x_{chol} = 0.50, whereas the reduction reported by Falck is 41% and that of Issack is 34%. Therefore, our calculated APL in DPPC/Chol systems seems to be overestimated by ≈8−23%, still in reasonable agreement considering the different Hamiltonians employed in the mentioned works.

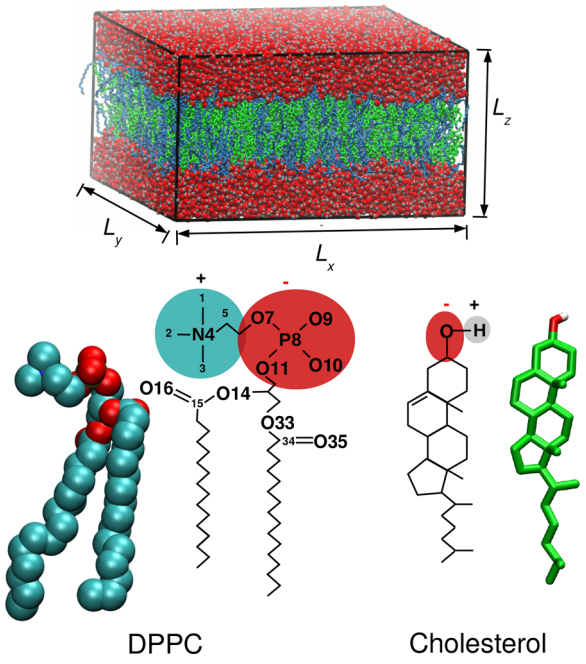

Figure 1. Top: Typical snapshot of an equilibrated DPPC/Chol bilayer with x_{chol} = 0.50. DPPC molecules are depicted in blue, Chol in green, and water oxygens in red. Bottom: Pictures and schemes of the molecular structures used in this work. In DPPC species, atom numbering from 1 to 11 reflects the head group specific sites.

Table 1. Composition of the Simulated Systems and Box Size Dimensions[a]

N_{DPPC}	N_{chol}	x_{chol}	A_{BOX}/nm^2	L_z/nm	APL (nm^2)
968	0	0.00	312.2	6.89	0.645
678	290	0.30	251.2	7.65	0.519
484	484	0.50	220.2	8.19	0.454

[a]In nanometers. The number of water molecules is N_w = 30 600 for all systems. In the last column, APL corresponds to the area per membrane component (DPPC+Chol) species.

3. RESULTS

3.1. Bilayer Structure. We will first examine the changes in the bilayer structure due to the inclusion of cholesterol. The

DOI: 10.1021/acs.jpcb.8b00360
J. Phys. Chem. B 2018, 122, 5897−5907

normalized density profiles along the direction normal to the bilayer, $\rho_\gamma(z)$, namely

$$\rho_\gamma(z) = \frac{1}{A_{BOX}} \left\langle \sum_i \delta(z_i^\gamma - z) \right\rangle \quad (1)$$

are shown in Figure 2. In the previous equation, $\langle \cdots \rangle$ denotes equilibrium average, z_i^γ represents the z-coordinate of γ-site (or

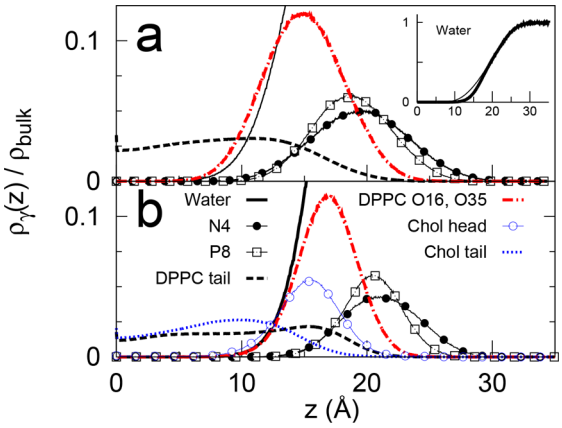

Figure 2. Water and lipid density distributions along the z-axis (with origin at the center-of-mass of the DPPC membrane). The plot represents the average of the two surfaces (upper and lower leaflet). Panels a and b correspond to the pure DPPC and x_{chol} = 0.50 membranes, respectively. The inset shows the water local density in a full scale.

the center-of-mass of a given moiety) in the ith molecule, and A_{BOX} is the box area. The average of the δ function in eq 1 is then simply the mean fluid density at position z. The plots in Figure 2 show local density profiles associated with water species, head/tail groups of DPPC and Chol, and some relevant sites of DPPC: nitrogen (N4) and phosphorus (P8), as representative of the head group conformations, and carbonyl oxygens (O16, O35). All the profiles have been normalized relative to the water bulk density, ρ_{bulk} = 0.033 Å^{-3}. Figure 2a corresponds to the pure DPPC membrane and Figure 2b to that with a Chol concentration of x_{chol} = 0.50.

The distribution of DPPC head groups in the pure DPPC bilayer may be obtained from $\rho_{P8}(z)$, taking the P8 site as representative of the whole head group. In the pure DPPC membrane, it is centered at z = 19 Å with a full width at half-maximum (fwhm) of Δz = 8 Å; in contrast, in the mixed bilayer containing x_{chol} = 0.50, the width shrinks down to Δz = 5.5 Å, along with a small shift of the head group peak toward more external locations ($z \approx 21$ Å). Moreover, the cholesterol molecules accommodate at deeper locations within the membrane, with the cholesterol head group peak located below the DPPC head groups, at $z \approx 15$ Å. The profiles reveal that the shorter Chol molecules become partly buried among the DPPC, with the Chol heads anchored at the level of the carbonyl groups of DPPC molecules, spanning a ~10 Å distance. Results from previous simulation studies[4,16,17,30] also show a thickening of the bilayer due to the addition of Chol, as revealed by a shift in the location of the DPPC head group peak toward the aqueous phase, being the magnitude of this effect determined by the Hamiltonian employed.

On the other hand, water molecules are mainly located at the interfacial and external regions of the membrane. The corresponding density shows a smooth increment along the z-axis, starting from inside the membrane, at z = 10 Å up to its bulk value at z = 25 Å. At greater distances, the water density looks constant and equal to the bulk density. Note that, in all cases, water molecules can be found below and above the position of the lipid head groups, penetrated into the lipid membrane up to the carbonyl group.

A more clear description of the local water density with respect to the positions of the DPPC head groups can be obtained by resorting to Voronoi tessellation procedure.[31] Briefly, this method involves the following steps: (i) the centers-of-mass of the DPPC head groups are brought to an arbitrary z' = 0 plane, by appropriate translations along the z-axis; (ii) the head groups are considered as centers of Voronoi cells which, in turn, define columnar sections along the z-axis; and (iii) at each time step, water molecules are associated with a unique Voronoi cell, whose center in the xy-plane lies closest

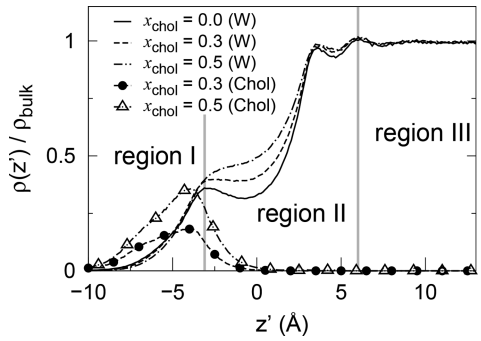

Figure 3. Densities of water (lines) and cholesterol heads (symbols) with respect to z' for different cholesterol compositions. The position z' = 0 corresponds now to the surface defined by DPPC head groups, obtained via a Voronoi tessellation procedure. Circles and triangles correspond to x_{chol} = 0.30 and 0.50, respectively. The profiles of Chol heads have been multiplied by a factor of 5 for better visualization.

to the tagged aqueous molecule. In Figure 3 we present profiles of the z'-dependence of water molecules, namely

$$\rho_\gamma(z') = \frac{1}{A_{BOX}} \left\langle \sum_i \delta(z_i^\gamma - z_{hg} - z') \right\rangle \quad (2)$$

The previous equation is similar to eq 1 except that, now, the sum is restricted to the water molecules lying within the Voronoi cell defined by the head group with z-coordinate z_{hg}. The new profiles are shown in Figure 3, normalized with the water bulk density, where we have also included the profiles of the Chol heads, with respect to the DPPC head group surface. Note that, in contrast to Figure 2, the water profiles do not appear as sigmoidal functions, since they represent "surface-to-particle" correlation functions.

Moreover, the aqueous profiles now have different structures, along three distinct regions. The first one (I) corresponds to z' values below the location of the first local maximum ($z' = -3.1$ Å) of the water density; the intermediate region (II) spans the interfacial range, where the aqueous density grows from $\rho(z') \approx \rho_{bulk}/2$ up to $\rho(z') \approx \rho_{bulk}$, at $z' = 6$ Å; finally, region III includes bulk waters and corresponds to a constant, uniform bulk density. Changes in the water profiles at different Chol contents are only detected in the interfacial region II, where an increment in the water density is observed with the addition of

DOI: 10.1021/acs.jpcb.8b00360
J. Phys. Chem. B 2018, 122, 5897−5907

cholesterol: note that around $z' = 0$, the aqueous density of the 1:1 DPPC/Chol membrane is nearly 50% larger than in the pure DPPC bilayer. When Chol molecules are inserted into the membrane, they localize at internal locations ($z' \sim -4$ Å); therefore, one would expect that the average distance between phospholipid head groups would increase. The average intermolecular distance between DPPC species on each leaflet (estimated as $d = \sqrt{A_{DPPC}}$, where $A_{DPPC} = A_{BOX}/(N_{DPPC}/2)$) yields $d = 8.0$ Å for the pure DPPC system, compared to $d = 9.5$ Å for $x_{chol} = 0.50$. These numbers reflect the spacing effect among DPPC head groups as the Chol concentration is increased; as a consequence, water molecules tend to fill the voids, and a local "water enrichment" occurs at the interfacial region.

Figure 4 shows a pictorial representation of the classification of water molecules in regions I–III for a typical configuration.

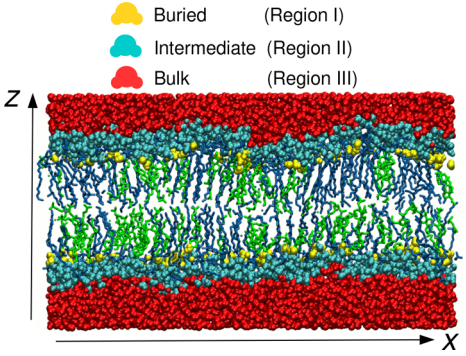

Figure 4. View of the DPPC/Chol hydrated membrane along the *xz*-plane ($x_{chol} = 0.5$). The water molecules have been classified according to their location with respect to the closest DDPC head group surface. Yellow, cyan, and red colors correspond to waters lying within regions I, II, and III, respectively.

The image corresponds to a system with $x_{chol} = 0.50$, and depicts the portion of the simulation box $|y| < 10$ Å. The complex rugosity of the interfacial region can be clearly perceived.

3.2. Dynamics. The dynamics of water and lipid molecules have been investigated by analyzing the time dependence of their lateral mean squared displacements (MSDs)

$$\mathcal{R}^2(t) = \langle |\mathbf{r}(t) - \mathbf{r}(0)|^2 \rangle \quad (3)$$

where $\mathbf{r}(t)$ is the projection of the center-of-mass position of molecules of a given type onto the *xy*-plane at time *t*.

In recent works, the diffusion of water species in hydrated lipid bilayers has been studied by neutron scattering techniques[32] and molecular dynamics simulations.[33,34] These investigations report an anomalous diffusion in the lateral motions of hydration water, on picosecond time scales. The computational results sketched in refs 33 and 34 show a subdiffusive dynamics for up to tens of picoseconds, that arises specifically from water molecules in the vicinity of phospholipid head groups at the interfacial region. A decreased long-time diffusion coefficient has also been observed in those works at the membrane interface, as compared with the usual value known for bulk water. These features are typical characteristics of obstructed diffusion in rough environments,[35,36] and have been explained in terms of the presence of hydrogen bonds between water and DPPC species and the heterogeneous energy landscape imposed by the phospholipid surface. By assuming a general power law dependence with time, $\mathcal{R}^2(t) \propto t^{\beta}$, we were able to obtain β from the logarithmic derivative of the MSD, from $\beta(t) = \partial \ln[\mathcal{R}^2(t)]/\partial \ln(t)$. The results yielded values of $\beta(t)$ corresponding to aqueous subdiffusive behavior ($\beta < 1$) on the picosecond time scale, in agreement with the data reported in refs 33 and 34 mentioned above; the corresponding plot is provided in the Supporting Information.

We are interested here in the spatial variation of the lateral diffusion coefficient of water along *z*. This was investigated following the procedure implemented in previous works.[37,38] Local diffusion coefficients of water, $D(z)$, were calculated as a function of the distance to the center of the membrane, according to a finite-difference expression of the type

$$D(z) = \frac{\mathcal{R}_z^2(t_2) - \mathcal{R}_z^2(t_1)}{4(t_2 - t_1)} \quad (4)$$

where the averages $\mathcal{R}_z^2(t)$ were accumulated in layers of rectangular bins of thickness $\Delta z = 2$ Å centered at *z*. The values t_1 and t_2 were fixed at 0.6 and 0.9 ns, respectively, on the assumption that the diffusional regime is reached after 0.6 ns (cf. Figure S2 in Supporting Information), and t_2 should be shorter than the actual residence time of water molecules within the considered bin. Since water molecules were assigned to a particular layer depending only upon their initial positions $\mathbf{r}(0)$, the physical meaning of the local diffusion coefficient that we compute is how fast solvent is leaving a given region of space.

Similar analysis can be extended to individual rotations, in a straightforward fashion.[38] In this case, local characteristic rotational times, $\tau_{rot}(z)$, were obtained from the time required for the local rotational correlation function, averaged in layers, to decay to 1/e. The local rotational correlation function was computed from the second-order Legendre correlation functions of the single dipole autocorrelation, $C_{2,z}(t) = \langle P_2[\boldsymbol{\mu}_{i,z}(t)\cdot\boldsymbol{\mu}_{i,z}(0)] \rangle$, with $\boldsymbol{\mu}_{i,z}$ being the dipolar unit vector of water molecules lying in the corresponding *z*-bin at $t = 0$, and $P_2(x)$ being the Legendre polynomial of second rank.

In Figure 5a we present the behavior of the lateral local water diffusivities $D(z)$; the rotational times $\tau_{rot}(z)$, normalized with

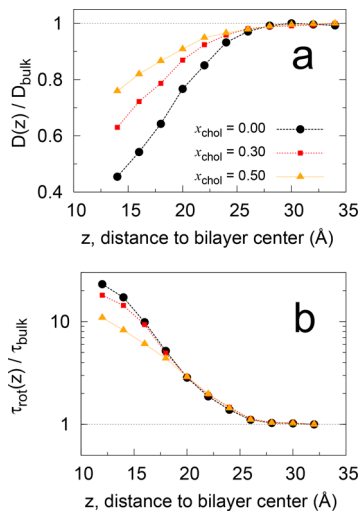

Figure 5. (a) Local diffusion coefficients and (b) rotational correlation times of water normalized with the corresponding bulk values, as a function of the distance to the center of the bilayer.

DOI: 10.1021/acs.jpcb.8b00360
J. Phys. Chem. B 2018, 122, 5897–5907

the corresponding bulk values, are shown in Figure 5b. The local diffusion coefficients are shown for $z > 12$ Å. At smaller distances, due to the slower and hindered mobility, the dynamics of water exhibits a subdiffusive behavior. Clearly, the lateral diffusion of water exhibits a sharp drop as one approaches the bilayer interface. This effect is less marked in the bilayer containing the highest cholesterol concentration than in the cholesterol-free case. In other words, we observe that the presence of cholesterol in the bilayer accelerates water translational mobility near the membrane interface.

In their experimental work, Cheng et al.[22] were able to determine translational correlation times of interfacial waters, τ_w, which are inversely proportional to local water diffusivities. The authors focused their attention on the biologically relevant Chol concentration and reported values of τ_w/τ_{bulk} for interfacial waters that drop from 6.9 down to 5.3 upon addition of 30 mol % Chol, resulting in a 23% reduction in the diffusive times. By considering that $\tau_w \propto D^{-1}$, this temporal reduction translates into a 30% increment in the interfacial diffusion coefficients. The experimental detection of the interfacial aqueous diffusivity is assumed to arise from water molecules lying within a 5−10 Å distance of the nitroxide radical-based spin label probes, which are attached to DPPC heads. In order to compare with experimental data, we have taken the average of the z-dependent local diffusivities $D(z)/D_{bulk}$ over 13 Å $\leq z \leq$ 22 Å, as the representative region of the DPPC heads location. We obtain in this way a more moderate increment in the aqueous diffusion, of ∼26%, at the same biological Chol concentration.

Similar features are observed in the rotational dynamics of water near the interfacial region, although the retardation effects are larger than those observed for lateral translations, leading to rotational relaxation ∼20 times slower than those found in bulk. Again, the retardations in the rotational times are smaller when cholesterol is added to the DPPC membrane, reducing the retardation factor, $\tau_{rot}(z)/\tau_{bulk}$, from 20 down to 10.

The dynamics of the lipid species in phospholipid membranes and the effects of cholesterol on their lateral diffusion have been previously investigated by NMR techniques[39] and molecular dynamics simulations.[30,40] As opposed to the interfacial water behavior, the experimental results show that the lipid lateral diffusion decreases linearly with increasing Chol concentration in the liquid disordered (l_d) phase, while the dependence on Chol is much weaker in the liquid ordered (l_o) phase. A quantitative comparison extracted from fluorescence correlation spectroscopy on DLPC/Chol membranes[41] shows that when the Chol concentration was incremented from 0 to 60%, the lateral diffusion coefficient of DLPC was reduced by a factor of 10. Although the computational results of Falck et al.[30] were obtained from DPPC/Chol systems, their findings are in reasonable agreement with the experimental data, and the reduction of the lateral diffusion with addition of cholesterol is explained in terms of the changes observed in the free area and free volume properties. In the present study, since our focus is put on interfacial waters, our 10 ns MD trajectories are still insufficient to obtain statistically reliable values of lipid diffusion coefficients. However, a rough estimation of lipid lateral diffusion can be computed from $D \sim \mathcal{R}^2(t)/4t$, considering the centers-of-mass of DPPC species in the calculation of the mean squared displacement. Our results, taken with care as just a rough guess, yielded lipid diffusion coefficients of the order of 10^{-8} cm^2/s, in accord with experiments[41] and previous computer simulations,[30] and exhibit a smaller reduction, by a factor of 2, when the Chol concentration is incremented from 0 to 50%. Plots of $\mathcal{R}^2(t)$ versus t and $\mathcal{R}^2(t)/4t$ versus t are provided in the Supporting Information.

The dynamical features of head and tail groups of atoms in DPPC lipids were also evaluated. The lateral mean squared displacements are shown in Figure 6a at different cholesterol concentrations. The calculation of the logarithmic slope of the MSD (Figure 6b) reveals that these lipid groups follow a subdiffusive dynamics in the time scales investigated here, below 10 ns. This subdiffusive lipid regime has been also reported in recent computer simulations on similar membranes.[33,42] From the analysis of long 100 ns MD trajectories the authors found a broad subdiffusive region, not present in simple fluids, that extends over a 10 ps $\leq t \leq$ 10 ns time scale, between the short time ballistic ($t \leq$ 10 fs) and the long time Fickian diffusion regime ($t \geq$ 30 ns). In the past, different models have been proposed to explain lipid dynamics based on diffusion in dense fluids. However, lipid molecules are polymers of specific flexibility and connectivity characteristics, and hence their lateral diffusion in bilayer systems is qualitatively different from the diffusion of molecules in dense fluids. We should also take into account the fact that the dynamics in the picosecond time scale depends strongly on the position of the atom within the lipid. The atoms at the end of the lipid tail have more freedom to move. Nevertheless, these atoms are also linked to the head group, which ultimately determine their diffusion on long time scales of the order of 30−100 ns. Under all the above considerations, a qualitative analysis of the behavior of the corresponding MSDs at different cholesterol concentrations, shown in Figure 6, reveals the following: (i) the lateral mobility of the head groups is faster than that of the tail groups in the time scale investigated; (ii) the addition of cholesterol to the DPPC membrane enhances the above difference, inducing faster mobilities of head groups and slower motions of tail groups, as compared with the cholesterol-free DPPC membrane. It is well-known that the addition of cholesterol produces structural ordering in a lipid membrane. The higher structural order associated with DPPC carbon chains is consistent with a slower tail group dynamics. On the other hand, cholesterol molecules are located deeper inside the membrane, buried below the DPPC head groups. As a result, the average intermolecular distance among DPPC head groups grows and the intermolecular head group interactions are

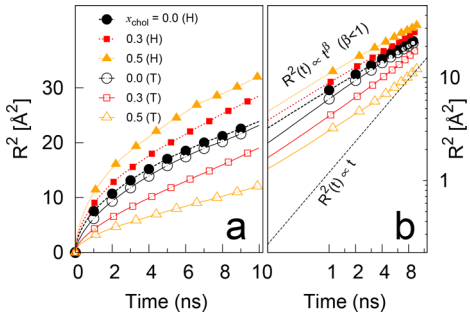

Figure 6. (a) Lateral mean squared displacement of heads and tails of DPPC molecules, for different concentrations of cholesterol. "H" and "T" refer to head and tail groups of DPPC species. Panel b shows the same curves in logarithmic scale, where the subdiffusive regime can be clearly seen in the investigated time scales.

DOI: 10.1021/acs.jpcb.8b00360
J. Phys. Chem. B 2018, 122, 5897−5907

weakened, resulting in less hindered motions, i.e., faster head group mobilities.

3.3. Hydrogen Bond Analysis. In addition to their contribution to the water−water hydrogen bond (HB) network, interfacial waters establish HBs with oxygen sites of lipid molecules. We have investigated the distribution and dynamics of these DPPC−water bonds, using a geometrical definition of the HB, similar to that employed by several authors in the literature.[33,43−45] Namely, an HB is defined between two molecules if the oxygen−oxygen distance (O···O) is less than 3.25 Å, and the angle between O···O and the corresponding O−H vector is no greater than 35°.

For the HB calculation we have considered 8 relevant oxygen atoms in DPPC molecules: phosphate oxygens O9, O10; carbonyl oxygens O16, O35; ether oxygens O7, O11, O14, and O33; and the hydroxyl moiety in the head group of Chol species. When computing the fraction of interfacial waters H-bonded to the different species in the membrane, we found that, at the higher Chol concentration studied, ∼90% of waters form HBs with DPPC and only a minimal fraction of ∼10%, with cholesterol. Therefore, we will consider only the most abundant water/DPPC bonds in the following discussion.

Figure 7 shows time averaged histograms of the HB probabilities, $P(n)$. The right panels of Figure 7 show that

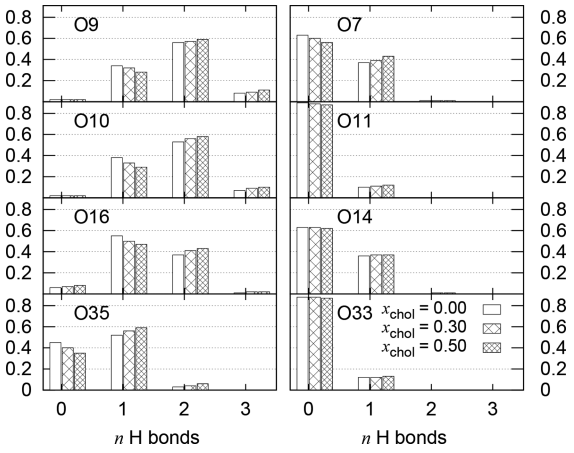

Figure 7. Probabilities ($P(n)$) of finding a number n of water/DPPC H-bonds per DPPC molecule, for different cholesterol concentrations. Left and right panels correspond to phosphate/carbonyl and ether oxygens of DPPC, respectively. The relative errors in the H-bond probabilities are of the order of 2−3%.

the probabilities of HB formation between ether oxygens of DPPC and water molecules are smaller than those corresponding to phosphate and carbonyl groups. Note that, due to their limited solvent accessibility, these ether oxygens are able to form a maximum of a single HB with water, with ≈40% probability in the cases of O7 and O14, and a lower chance, of ≈10%, in the cases of O11 and O33. In agreement with previous works,[4,33,46,47] we found that the phosphate and carbonyl oxyens have higher probabilities of establishing HBs than ether oxygens. A major fraction of DPPC/water HBs involves the head group oxygens O9 and O10. These are, in turn, the most accessible to hydration waters, via multiple HBs.

The variations of the probabilities $P(n)$ with Chol concentration show a tendency favoring the formation of DPPC/water HBs with increasing x_{chol}. More specifically, there is a 5−15% increment in the probability of forming two HBs in going from x_{chol} = 0 to x_{chol} = 0.50. This feature is consistent with the increment of the water local densities at the interfacial region with addition of Chol, observed in Figure 3. The total average number of water/lipid HBs per lipid can be obtained by performing the sum

$$\langle n_{HB} \rangle = \sum_n nP(n) \tag{5}$$

The results are listed in the second column of Table 2.

In order to classify and understand the HB structure between DPPC lipids and water at the membrane interface, we started by analyzing the H-bonds Y···H−O−H, where Y represents any of the eight relevant oxygen sites in DPPC species mentioned above. After having classified all DPPC/water HBs, we analyzed the identity of the other HB acceptor site "X", in a Y···H− O−H···X arrangement. As such, we have classified the DPPC/water H-bonds in two categories: (i) There are arrangements of the type Y···H−O−H···O_w, in which a tagged water is connected with DPPC and a second water at the same time. We will refer to this type of bond as LWW, meaning lipid/water/water (Figure 8a). (ii) A water molecule forms

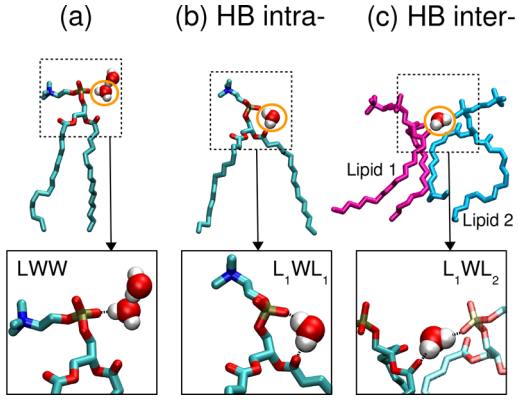

Figure 8. Snapshots of the different types of HBs that may be found between DPPC and water molecules. The structure shown in part a corresponds to a single HB between DPPC and water, whereas in parts b and c, water forms two HBs with DPPC: the configuration shown in part b corresponds to intralipid (L_1WL_1) bridge bonds, whereas that in part c corresponds to interlipid ones (L_1WL_2).

Table 2. Average Number of DPPC/Water H-Bonds per DPPC Molecule ($\langle n_{HB} \rangle$) and Fraction of H-Bonds of Types LWW and LWL[a]

x_{chol}	$\langle n_{HB} \rangle$	x_{LWW}	$x_{L_1WL_1}$	$x_{L_1WL_2}$
0.00	5.70 ± 0.04	0.764 ± 0.009	0.025 ± 0.002	0.211 ± 0.007
0.30	5.97 ± 0.05	0.811 ± 0.011	0.025 ± 0.003	0.164 ± 0.008
0.50	6.38 ± 0.06	0.855 ± 0.012	0.026 ± 0.004	0.119 ± 0.008

[a]The latter are decomposed into intralipid (L_1WL_1) and interlipid (L_1WL_2) bonds.

DOI: 10.1021/acs.jpcb.8b00360
J. Phys. Chem. B 2018, 122, 5897−5907

simultaneously two HBs with DPPC species, corresponding to a structure of the type: Y···H−O−H···X, where Y and X denote different oxygen sites in DPPC species. This type of bond will be denoted as lipid/water/lipid (LWL) ones. In turn, these LWL bonds can be found in two categories: (a) water is H-bonded to two different oxygens of the *same* lipid molecule, in such a way that an intralipid water bridge is formed (L_1WL_1, Figure 8b); or (b) water is H-bonded to two *different* DPPC lipids, forming a so-called interlipid water bridge (L_1WL_2, Figure 8c). All of these typical configurations for DPPC/water hydrogen bonds are illustrated in Figure 8.

The resulting averaged fractions for each type of HB, with respect to the total number of DPPC/water bonds, are listed in Table 2 for the studied systems.

Although the average $\langle n_{HB} \rangle$ increases upon the addition of cholesterol, we found that the fraction of HBs of the type L_1WL_1 remains constant and equal to 2.5%, regardless of the Chol concentration, whereas the fraction of L_1WL_2 bonds decreases with x_{chol}. In fact, in the pure DPPC membrane, ∼20% of the HBs arise from waters connecting two different lipids, whereas the percentage reduces roughly to the half at $x_{chol} = 0.50$. The above numbers suggest a scenario in which the addition of cholesterol induces a rupture of interlipid water bonds of type L_1WL_2 and a transformation into simple DPPC/water bonds of type LWW. In Section 3.1 we noticed that the addition of Chol at 50 mol % concentration produces a slight 1.5 Å increment in the average intermolecular distance among DPPC head groups. The changes observed in the water/lipid HB network suggest that this variation is sufficient to drive the rupture of a substantial fraction of interlipid water bridge H-bonds.

Before closing the statistical study of the different types of HBs, in Figure 9 we show the populations of LWW and LWL

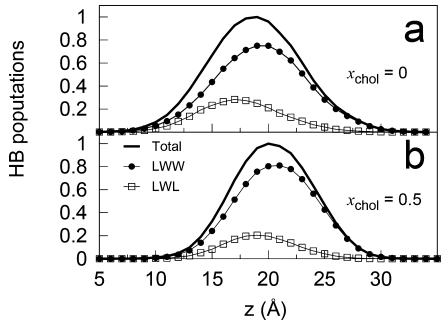

Figure 9. Hydrogen bond populations as a function of the location of the associated aqueous oxygen atom, along the *z*-axis. The histograms represent the average of the two membrane surfaces (upper and lower leaflet) and were normalized to the maximum value of the curves corresponding to the total population of DPPC/water H-bonds. The relative errors are on the order of 2−3%.

bonds as a function of the location of their associated aqueous oxygen. We only display the curves obtained for two systems: the pure DPPC membrane (Figure 9a) and that with x_{chol} = 0.50 (Figure 9b). At first glance, we notice that all curves are shifted toward larger values of *z* with the addition of Chol, reflecting the shift of the local density of DPPC head groups toward more external locations, already observed in Figure 2. The plot also shows that, in both systems, the LWL type of HBs is located deeper than the LWW ones, within the membrane. Most notable is the change in the relative intensities of the peak heights. With the addition of Chol, the population of LWW increases while that of LWL bonds decreases. More specifically, the major drop in the LWL population seems to occur on the left-hand side of the band (around 15 Å ≤ *z* ≤ 17 Å), coinciding with the region where Chol head groups are localized, and therefore, where Chol−water bonds could be found. The variations observed in the bond populations suggest, then, that the addition of Chol produces the rupture of a substantial number of LWL hydrogen bonds that may be replaced in part by Chol/water ones. Since the region mentioned above is occupied also by the DPPC head groups (see Figure 2), and is characterized by a significant increment in the water local density when Chol is added, we investigated the number of HBs between water species arising from water molecules that lie within the interfacial region (region II of Figure 3). We found that the presence of cholesterol promotes an increment in the average number of water/water H-bonds per molecule, $\langle n_{HB}^{ww} \rangle$. Specifically, we obtained the values of $\langle n_{HB}^{ww} \rangle$ = 1.85, 1.97, and 2.07 for x_{chol} = 0, 0.30, and 0.50, respectively, indicating a 12% increment in the number of HBs between interfacial waters when 50 mol % of Chol is incorporated into the membrane.

The dynamics of the DPPC/water hydrogen bonds may be evaluated through the time correlation function of the instantaneous occupation numbers,[48,49] $\eta_{ij}(t)$. These variables take the value 0 or 1 depending on the H-bonding state of each *ij* pair of molecules, that is

$$\eta_{ij}(t) = \begin{cases} 1 & \text{if molecules } i \text{ and } j \text{ are H-bonded} \\ 0 & \text{otherwise} \end{cases} \quad (6)$$

The probability that an H-bond, which was intact at the initial time, remains alive at time *t* is then represented by the normalized autocorrelation function of η_{ij}, averaged over all *ij* pairs, namely

$$C_{HB}(t) = \langle \eta_{ij}(0)\eta_{ij}(t) \rangle \quad (7)$$

These functions are displayed in Figure 10 for the systems with different cholesterol content.

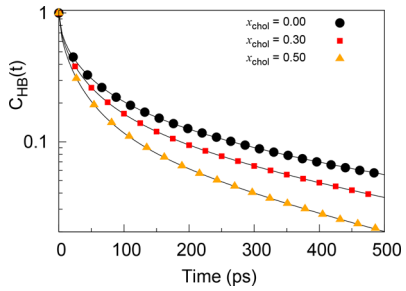

Figure 10. Hydrogen bond autocorrelation function, $C_{HB}(t)$, of DPPC/water bonds obtained for the systems studied. Symbols correspond to the computed functions and lines, to the corresponding best fitting functions (see eq 8).

We notice that $C_{HB}(t)$ decays faster with increasing Chol concentration. This reduction of the DPPC/water hydrogen bond relaxation times with the addition of cholesterol is concomitant with the faster dynamical behavior of water displayed in Figure 5. Diffusion and reorientations are dynamic properties associated with single-molecule motions, however, they are to a large extent manifestations of the underlying dynamics of the whole H-bond network. Looking for a physical

DOI: 10.1021/acs.jpcb.8b00360
J. Phys. Chem. B 2018, 122, 5897−5907

interpretation of this dynamical variation, we analyze a very simple scheme, that considers a two-state model for $C_{HB}(t)$. Within this framework, we assume that $C_{HB}(t)$ contains contributions from (i) the HBs arising from waters forming only one bond with a DPPC molecule (LWW like), relaxing with a fast time scale τ_1, and (ii) HBs arising from waters forming two bonds with DPPC molecules, through intra- or interlipid bridging waters (LWL bonds), described by a slower time scale τ_2. The global autocorrelation functions can be well-described by a superposition of two, fast and slow, stretched exponential functions of the type

$$C_{HB}(t) \approx a_1 e^{-(t/\tau_1)^{\beta_1}} + a_2 e^{-(t/\tau_2)^{\beta_2}} \quad (8)$$

where β_i is the stretching exponent, a dimensionless parameter that modifies the shape of the exponential function $\exp(-t/\tau_i)$ by stretching it when $0 < \beta < 1$. The characteristic HB lifetime, τ_{HB}, can be obtained from time integrals of the correlation function, thus resulting in

$$\tau_{HB} = \int_0^\infty C_{HB}(t)\, dt = \frac{a_1\tau_1}{\beta_1}\Gamma(1/\beta_1) + \frac{a_2\tau_2}{\beta_2}\Gamma(1/\beta_2) \quad (9)$$

where Γ is the gamma function.

On the basis of the two-state model mentioned above, the partial weights of the two contributions of the fitting function (a_1 and a_2 in eq 8) were forced to be fixed and equal to the fraction of H-bonds arising from waters forming one and two HBs with DPPC species (i.e., x_{LWW} and $x_{LWL} = x_{L_1WL_1} + x_{L_1WL_2}$ of Table 2).

Figure 10 shows the computed correlation functions $C_{HB}(t)$ and the corresponding fitting functions imposing the constraints mentioned above; the best fitting parameters are displayed in Table 3, along with the HB lifetimes τ_{HB}.

Table 3. Stretched-Exponential Fitting Parameters to $C_{HB}(t)$ for DPPC/Water Pairs at Different Concentrations, and H-Bond Typical Relaxation Times Obtained from Time Integrals of the Fitting Functions[a]

	H-bond correlation function						
x_{chol}	a_1	τ_1	β_1	a_2	τ_2	β_2	τ_{HB}
0.00	0.764	18.8	0.547	0.236	270.3	0.654	111.7
0.30	0.811	16.8	0.558	0.189	261.7	0.738	79.7
0.50	0.855	13.8	0.582	0.145	213.6	0.787	56.6

[a]Times are given in picoseconds.

We observe that the fast component, with amplitude a_1, has a characteristic time τ_1 of the order of tens of picoseconds. Note that this time scale is yet 10 times slower than the typical HB relaxation time of water/water bonds in bulk water, which is of the order of $\tau_{HB} \approx 1-5$ ps.[45] The slowest contribution exhibits typical time scales of $\tau_2 \approx 200$ ps, consistent with a slower librational dynamics, that can be associated with the double bridging role of the involved waters connecting two massive lipid molecules.

A detailed analysis of the fitting parameters listed in Table 3 shows that τ_1 and τ_2 values are progressively smaller with increasing Chol concentrations, with τ_1, τ_2 being ~20−25% faster at $x_{chol} = 0.50$ than in the pure DPPC system. The optimal stretching exponent parameters were found to be smaller than unity and did not exhibit relevant variations with x_{chol}. Due to the increment of the relative weight of the fast contribution with increasing Chol concentration, the global HB lifetime associated with the $x_{chol} = 0.50$ system, of $\tau_{HB} = 56.6$ ps, was only one-half of that corresponding to the pure DPPC membrane, $\tau_{HB} = 111.7$ ps.

The good agreement obtained for the fitting procedure, and the magnitudes of the optimal τ_1 and τ_2, well-separated in time, would confirm that the simple two-state model considered here provides a valid physical interpretation for the aqueous H-bond dynamics at the membrane interface.

3.4. Translational Order and Excess Entropy. Motivated by the above observations, we investigated the translational order parameter χ_t, defined as[50,51]

$$\chi_t = \frac{1}{\xi_c}\int_0^{\xi_c} |g(\xi) - 1| d\xi \quad (10)$$

where $g(\xi)$ is the pair correlation function, $\xi = r\rho^{1/3}$ represents the radial distance expressed in units of the mean intermolecular separation, and ξ_c is a numerical cutoff. This order metric provides a measure of the tendency of pairs of molecules to be separated by preferential distances, over a finite number of coordination shells. In the past, this magnitude has been used to investigate Lennard-Jones systems,[52] thermodynamic anomalies in liquid silica,[50] and colloidal systems as well.[53] Note that the translational order parameter vanishes for an ideal gas ($g = 1$), whereas it can be relatively large for crystal structures or systems with long-range order.

Another interesting statistical quantity that can be measured in the simulation is the excess entropy, $s^{exc} = s - s^{id}$, defined as the difference between the total entropy of a real fluid and the entropy of an ideal gas (s^{id}), at the same temperature and density. The excess entropy can be estimated from the two-body contribution to the expansion of the total excess entropy in terms of multiparticle correlations. Therefore, in terms of the radial pair distribution function, $s_{exc}^{(2)}$ can be written as[54−56]

$$\frac{s_{exc}^{(2)}}{k_B} = -\frac{\rho}{2}\int \{g(r)\ln g(r) - [g(r) - 1]\} d\mathbf{r} \quad (11)$$

When truncated at the two-body terms, the series has been shown to be a reasonable approximation for the full excess entropy in several model liquids.[57,58] $s_{exc}^{(2)} = 0$ for completely disordered systems (i.e., the ideal gas) and becomes large and negative for ordered structures. As such, it provides a practical measure of disorder in the system. In the context of the present paper, in which our interest was focused on the interfacial layer, we computed the lateral radial distribution function, $g_{\parallel}$, over the xy-plane, and introduced it in eqs 10 and 11. We considered a thin slab of thickness $\delta z = 2$ Å and area A_{BOX}, centered at a tagged aqueous oxygen located in region II (see Figure 3), and only the water pairs whose oxygen sites lie both within that slab were taken into account for the calculation.

Our results, summarized in Table 4, reveal that the translational order of liquid water near the membrane interface

Table 4. Translational Order Parameter and Excess Entropy for Interfacial Water and DPPC Head Groups

	water		DPPC head groups	
x_{chol}	χ_t	s^{exc}/k_B	χ_t	s^{exc}/k_B
0.00	0.129	−2.16	0.213	−0.605
0.30	0.112	−1.97	0.202	−0.571
0.50	0.108	−1.84	0.190	−0.510

DOI: 10.1021/acs.jpcb.8b00360
J. Phys. Chem. B 2018, 122, 5897−5907

decreases with the addition of cholesterol, from $\chi_t = 0.129$ for the pure DPPC membrane down to $\chi_t = 0.108$ for the 1:1 DPPC/Chol mixed one. With a similar calculation, the result for the translational order parameter of the DPPC head groups exhibits the same trend: it decreases from $\chi_t = 0.213$ for $x_{chol} = 0$ to $\chi_t = 0.193$ for $x_{chol} = 0.5$.

Although the differences found in $s_{exc}^{(2)}$ are relatively small (≈15% reduction in magnitude), the values for the excess entropy of interfacial waters show that $s_{exc}^{(2)}$ becomes less negative with the addition of cholesterol, indicating that the presence of cholesterol within the membrane induces more disorder in the neighboring water molecules, compared to water near a pure DPPC membrane. Moreover, the excess entropy associated with the DPPC head groups has the same tendency, suggesting that the lipid external surface tends to exhibit a more disordered structure as cholesterol is incorporated in the membrane.

4. CONCLUSIONS

In this paper, we investigated the effects of cholesterol on the dynamics of interfacial waters in phospholipid bilayer membranes, by means of molecular dynamics simulations. To that end, we investigated a fully hydrated DPPC membrane containing mole fractions of cholesterol of 0.30 and 0.50, at a temperature of 323 K.

As a first step we analyzed the effects of cholesterol on the structure of the membrane. This analysis was based on the computation of the area per lipid and density profiles. The former yielded a 30% reduction in the APL upon addition of 50 mol % of cholesterol, in good agreement with previous experimental and computational data. Local density profiles along the direction perpendicular to the membrane surface were computed for the different species, revealing a thickening of the bilayer. A Voronoi tessellation procedure allowed us to classify the water molecules hydrating the membrane into three distinct regions, containing (i) buried waters below the head group surface, (ii) interfacial waters solvating the lipid head groups, and (iii) bulk-like waters. In accord with the findings of Falck et al.,[30,40] that support the reduction of the total free volume with an increasing cholesterol content, we observe an increment in the local density of water at the interfacial region with the addition of Chol.

The analysis of the dynamics of the interfacial waters revealed that the inclusion of cholesterol to DPPC membranes modifies the aqueous dynamics: water molecules diffuse faster, their rotational relaxation times are shorter, and the DPPC/water hydrogen bond dynamics relaxes faster than in the pure DPPC membrane. The observed acceleration of the lateral translational water mobility at the interface is in agreement with experimental results performed recently by Cheng et al.,[22] obtained by means of NMR techniques. The experiments report a 23% reduction in the diffusive times of interfacial waters upon addition of 30 mol % of cholesterol, whereas in this work we obtained a slightly more moderate reduction of aqueous diffusive times, of 20%. The analysis of the rotational mobility of interfacial waters revealed that their orientational dynamics was also affected by the addition of cholesterol, yielding smaller relaxation times in the presence of cholesterol. Although diffusion and reorientations are dynamic properties associated with single-molecule motions, they are certainly manifestations of the underlying dynamics of the hydrogen bond network.

The hydrogen bond dynamics of DPPC/water bonds was evaluated by calculating appropriate time correlation functions. We have first classified the DPPC/water hydrogen bonds into two categories, according to the identity of the other H-bond of each bonded water: (i) fast and mobile HBs, arising from waters bonded to a DPPC molecule and to another water molecule (LWW states); and (ii) more rigid and slower H-bonds, arising from waters that form simultaneously two donor hydrogen bonds with DPPC species (LWL states). The global time correlation function associated with DPPC/water bonds exhibited a faster decay with increasing Chol concentrations. On the basis of the above distinction among different H-bonds, the faster relaxation of the total TCF can be cast in terms of a simple two-state model, assuming that the TCF contains two contributions, a fast one accounting for LWW states and a slow component associated with LWL bonding states. In agreement with the proposed two-state model, two characteristic times were found, well-separated in time. The relative weight of the slow contribution ($\tau_2 \sim 250$ ps), associated with the population of LWL bonds, decreases with the addition of cholesterol, whereas that of the fast component ($\tau_1 \sim 15$ ps) increases. This can be understood in terms of the augmented interfacial water density with cholesterol, that leads to a greater competition to form hydrogen bonds with other waters, producing a rupture of a substantial number of interlipid LWL bonds, at the expense of the formation of LWW new ones.

Before closing the hydrogen bond dynamics discussion, we would like to address a comment about the use of stretched exponentials to fit the HB correlation function. In fact we have first tried to fit the HB correlations with a typical sum of two or three exponentials, with no success. The fact that a stretched exponential function can fit data very well over many orders of magnitude suggests, but by no means proves, that it must be of some fundamental significance. However, there is probably not a unique model explaining the presence of the stretched relaxation in all cases. Just to mention a couple of examples, we note that Fogarty and Laage show, in their computational study of water dynamics in protein hydration shells,[59] that a stretched exponential function appears to give a reasonable fit of the reorientational correlation function; however, the corresponding probability distribution of relaxation times (i.e., the Laplace transform of the time decay) bears no resemblance to the distribution calculated explicitly from the simulations. Therefore, they conclude that a stretched exponential should only be regarded as a fit without any physical meaning. Gnanasekaran and co-workers also found, in their computational study of interfacial waters in a dimeric hemoglobin,[60] that the water−protein hydrogen bond correlation function is well-described by stretched exponentials with exponents between 0.1 and 0.6. On the other hand, Rezus and Bakker found that bi- and triexponential decays are able to accurately fit the decay of molecular reorientation of water in their femtosecond spectroscopy experiments on hydrophobic hydration.[61] Similar findings have been reported from computer simulation studies as well.[62] By mentioning these few examples, it is clear that it is a nontrivial issue, and although the presence of stretched relaxation is usually linked to dynamic heterogeneity, a concept often used in glassy systems, reports from different works remain contradicting, and the issue remains unresolved. In our case, we believe that the presence of stretched exponential relaxations in HB dynamics of hydration waters might be related to a broad correlation time distribution, caused by the heterogeneity and complexity of the membrane surface, which

DOI: 10.1021/acs.jpcb.8b00360
J. Phys. Chem. B 2018, 122, 5897−5907

leads to slower hydrogen bond rearrangements and steric hindrance to water mobility.

We have finally estimated the excess entropy of the investigated systems, based on the two-body contribution to the expansion of the total excess entropy. Although the variations obtained in the excess entropy as a function of Chol concentration are relatively small, we found that the excess entropy of interfacial waters becomes less negative whith the addition of Chol, indicating more disorder.

In summary, it could be stated that the addition of cholesterol leads to a reduction in the average free area within the membrane and promotes the appearance of a more dense aqueous phase at the interface. As a consequence, a fraction of the slow and "opened" LWL interlipid-like H-bonds are broken at the expense of the formation of new and more compact LWW bonds. The latter are faster and more mobile, leading to an enhancement in the water mobility at the interface. An additional contribution to the water dynamics enhancement may likely arise from the larger fraction of fast water/water H-bonds at the interface, a fact that can be inferred from the increment of the local water density at the membrane interfacial region.

As such, in a broader context, the presence of Chol in the phospholipid membrane would possibly act as a "facilitator" of the interactions between the membrane and other biological constituents, such as proteins or ligands, by means of the disruption of strong and rigid LWL hydrogen bonds, at the expense of the formation of weaker and more mobile LWW bonds. The faster mobility observed in surface waters may eventually facilitate the approach of biological constituents to the membrane. In general, cholesterol is found in plasma membranes at typical molar fractions of 30−40%; therefore, the physical properties described in this work would be relevant in determining the functional effects of Chol on biological lipid membranes.

■ ASSOCIATED CONTENT

Supporting Information

The Supporting Information is available free of charge on the ACS Publications website at DOI: 10.1021/acs.jpcb.8b00360.

Lateral mean squared displacement of water within Voronoi regions, lateral mean squared displacement of water within layered rectangular bins for local diffusivities, and lateral mean squared displacement of DPPC species (PDF)

■ AUTHOR INFORMATION

Corresponding Author

*E-mail: DoloresElola@gmail.com. Phone: +54 11 6772 7046. Fax: +54 11 6772 7121.

ORCID

M. Dolores Elola: 0000-0001-5014-190X

Notes

The authors declare no competing financial interest.

■ ACKNOWLEDGMENTS

M.D.E. and J.R. acknowledge financial support from ANPCyT (Grant PICT 2013-1323) and CONICET (Grant PIP 112-201501-00417). M.D.E. and J.R. are staff members of CONICET, Argentina.

■ REFERENCES

(1) Bloom, M.; Evans, E.; Mouritsen, O. G. Physical Properties of the Fluid Lipid-Bilayer Component of Cell Membranes: A Perspective. *Q. Rev. Biophys.* **1991**, *24*, 293−397.

(2) Nagle, J. F.; Tristram-Nagle, S. Structure of Lipid Bilayers. *Biochim. Biophys. Acta, Rev. Biomembr.* **2000**, *1469*, 159−195.

(3) van Meer, G.; Voelker, D. R.; Feigenson, G. W. Membrane Lipids: Where They Are and How They Behave. *Nat. Rev. Mol. Cell Biol.* **2008**, *9*, 112−124.

(4) Róg, T.; Pasenkiewicz-Gierula, M.; Vattulainen, I.; Karttunen, M. Ordering Effects of Cholesterol and its Analogues. *Biochim. Biophys. Acta, Biomembr.* **2009**, *1788*, 97−121.

(5) Tieleman, D. P.; Marrink, S. J.; Berendsen, H. J. C. A Computer Perspective of Membranes: Molecular Dynamics Studies of Lipid Bilayer Systems. *Biochim. Biophys. Acta, Rev. Biomembr.* **1997**, *1331*, 235−270.

(6) Saiz, L.; Bandyopadhyay, S.; Klein, M. L. Towards an Understanding of Complex Biological Membranes from Atomistic Molecular Dynamics Simulations. *Biosci. Rep.* **2002**, *22*, 151−173.

(7) Smondyrev, A. M.; Berkowitz, M. L. Molecular Dynamics Simulation of the Structure of Dimyristoylphosphatidylcholine Bilayers with Cholesterol, Ergosterol, and Lanosterol. *Biophys. J.* **2001**, *80*, 1649−1658.

(8) Feller, S. E. Molecular Dynamics Simulations of Lipid Bilayers. *Curr. Opin. Colloid Interface Sci.* **2000**, *5*, 217−223.

(9) Scott, H. L. Modeling the Lipid Component of Membranes. *Curr. Opin. Struct. Biol.* **2002**, *12*, 495−502.

(10) Issack, B. B.; Peslherbe, G. H. Effects of Cholesterol on the Thermodynamics and Kinetics of Passive Transport of Water through Lipid Membranes. *J. Phys. Chem. B* **2015**, *119*, 9391−9400.

(11) Oldfield, E.; Meadows, M.; Rice, D.; Jacobs, R. Spectroscopic Studies of Specifically Deuterium Labeled Membrane Systems. Nuclear Magnetic Resonance Investigation of the Effects of Cholesterol in Model Systems. *Biochemistry* **1978**, *17*, 2727−2740.

(12) Urbina, J. A.; Pekerar, S.; Le, H.-b.; Patterson, J.; Montez, B.; Oldfield, E. Molecular Order and Dynamics of Phosphatidylcholine Bilayer Membranes in the Presence of Cholesterol, Ergosterol and Lanosterol: A Comparative Study Using ^{2}H-, ^{13}C- and ^{31}P-NMR Spectroscopy. *Biochim. Biophys. Acta, Biomembr.* **1995**, *1238*, 163−176.

(13) Marsh, D.; Smith, C. P. An Interacting Spin Label Study of the Fluidising and Condensing Effects of Cholesterol on Lecithin Bilayers. *Biochim. Biophys. Acta, Biomembr.* **1973**, *298*, 133−144.

(14) Boggs, J. M.; Hsia, J. C. Effect of Cholesterol and Water on the Rigidity and Order of Phosphatidylcholine Bilayers. *Biochim. Biophys. Acta, Biomembr.* **1972**, *290*, 32−42.

(15) Mitchell, D. C.; Litman, B. J. Effect of Cholesterol on Molecular Order and Dynamics in Highly Polyunsaturated Phospholipid Bilayers. *Biophys. J.* **1998**, *75*, 896−908.

(16) Smondyrev, A. M.; Berkowitz, M. L. Structure of Dipalmitoylphosphatidylcholine/Cholesterol Bilayer at Low and High Cholesterol Concentrations: Molecular Dynamics Simulation. *Biophys. J.* **1999**, *77*, 2075−2089.

(17) Hofsäß, C.; Lindahl, E.; Edholm, O. Molecular Dynamics Simulations of Phospholipid Bilayers with Cholesterol. *Biophys. J.* **2003**, *84*, 2192−2206.

(18) Yeagle, P. L. Cholesterol and the Cell Membrane. *Biochim. Biophys. Acta, Rev. Biomembr.* **1985**, *822*, 267−287.

(19) Finean, J. B. Interaction between Cholesterol and Phospholipid in Hydrated Bilayers. *Chem. Phys. Lipids* **1990**, *54*, 147−156.

(20) Ohvo-Rekilä, H.; Ramstedt, B.; Leppimäki, P.; Slotte, J. P. Cholesterol Interacions with Phospholipids in Membranes. *Prog. Lipid Res.* **2002**, *41*, 66−97.

(21) Marquardt, D.; Kucerka, N.; Wassall, S. R.; Harroun, T. A.; Katsaras, J. Cholesterol's Location in Lipid Bilayers. *Chem. Phys. Lipids* **2016**, *199*, 17−25.

(22) Cheng, C.-Y.; Olijve, L. L. C.; Kausik, R.; Han, S. Cholesterol Enhances Surface Water Diffusion of Phospholipid Bilayers. *J. Chem. Phys.* **2014**, *141*, 22D513.

DOI: 10.1021/acs.jpcb.8b00360
J. Phys. Chem. B 2018, 122, 5897−5907

(23) Nagle, J. F.; Zhang, R.; Tristram-Nagle, S.; Sun, W.; Petrache, H. I.; Suter, R. M. X-Ray Structure Determination of Fully Hydrated L_α Phase Dipalmitoylphosphatidylcholine Bilayers. *Biophys. J.* **1996**, *70*, 1419−1431.
(24) Chiu, S. W.; Clark, M.; Balaji, V.; Subramaniam, S.; Scott, H. L.; Jakobsson, E. Incorporation of Surface Tension into Molecular Dynamics Simulation of an Interface: A Fluid Phase Lipid Bilayer Membrane. *Biophys. J.* **1995**, *69*, 1230−1245.
(25) Phillips, J. C.; Braun, R.; Wang, W.; Gumbart, J.; Tajkhorshid, E.; Villa, E.; Chipot, C.; Skeel, R. D.; Kale, L.; Schulten, K. Scalable Molecular Dynamics with NAMD. *J. Comput. Chem.* **2005**, *26*, 1781−1802.
(26) Darden, T. A.; York, D. M.; Pedersen, L. G. Particle Mesh Ewald - An N.log(N) Method for Ewald Sums in Large Systems. *J. Chem. Phys.* **1993**, *98*, 10089.
(27) Patra, M.; Karttunen, M.; Hyvönen, M. T.; Falck, E.; Vattulainen, I. Lipid Bilayers Driven to a Wrong Lane in Molecular Dynamics Simulations by Subtle Changes in Long-Range Electrostatic Interactions. *J. Phys. Chem. B* **2004**, *108*, 4485−4494.
(28) Sum, A. K.; de Pablo, J. J. Molecular Simulation Study on the Influence of Dimethylsulfoxide on the Structure of Phospholipid Bilayers. *Biophys. J.* **2003**, *85*, 3636−3645.
(29) Patra, M.; Karttunen, M.; Hyvönen, M. T.; Falck, E.; Lindqvist, P.; Vattulainen, I. Molecular Dynamics Simulations of Lipid Bilayers: Major Artifacts Due to Truncating Electrostatic Interactions. *Biophys. J.* **2003**, *84*, 3636−3645.
(30) Falck, E.; Patra, M.; Karttunen, M.; Hyvönen, M. T.; Vattulainen, I. Lessons of Slicing Membranes: Interplay of Packing, Free Areas, and Lateral Diffusion in Phospholipids/Cholesterol Bilayers. *Biophys. J.* **2004**, *87*, 1076−1091.
(31) Pandit, A.; Bostick, D.; Berkowitz, M. L. An Algorithm to Describe Molecular Scale Rugged Surfaces and its Application to the Study of a Water/Lipid Bilayer Interface. *J. Chem. Phys.* **2003**, *119*, 2199−2205.
(32) Toppozini, L.; Roosen-Runge, F.; Bewley, R. I.; Dalgliesh, R. M.; Perring, T.; Seydel, T.; Glyde, H. R.; Garcia Sakai, V.; Rheinstädter, M. C. Anomalous and Anisotropic Nanoscale Diffusion of Hydration Water Molecules in Fluid Lipid Membranes. *Soft Matter* **2015**, *11*, 8354−8371.
(33) Das, J.; Flenner, E.; Kosztin, I. Anomalous Diffusion of Water Molecules in Hydrated Lipid Bilayers. *J. Chem. Phys.* **2013**, *139*, 065102.
(34) von Hansen, Y.; Gekle, S.; Netz, R. R. Anomalous Anisotropic Diffusion Dynamics of Hydration Water at Lipid Membranes. *Phys. Rev. Lett.* **2013**, *111*, 118103.
(35) Szymanski, J.; Weiss, M. Elucidating the Origin of Anomalous Diffusion in Crowded Fluids. *Phys. Rev. Lett.* **2009**, *103*, 038102.
(36) Malchus, N.; Weiss, M. Anomalous Diffusion Reports on the Interaction of Misfolded Proteins with the Quality Control Machinery in the Endoplasmic Reticulum. *Biophys. J.* **2010**, *99*, 1321−1328.
(37) Lounnas, V.; Pettitt, B. M.; Phillips, G. N., Jr A Global Model of the Protein-Solvent Interface. *Biophys. J.* **1994**, *66*, 601−614.
(38) Lee, S. L.; Debenedetti, P. G.; Errington, J. R. A Computational Study of Hydration, Solution Structure, and Dynamics in Dilute Carbohydrate Solutions. *J. Chem. Phys.* **2005**, *122*, 204511.
(39) Filippov, A.; Orädd, G.; Lindblom, G. The Effect of Cholesterol on the Lateral Diffusion of Phospholipids in Oriented Bilayers. *Biophys. J.* **2003**, *84*, 3079−3086.
(40) Falck, E.; Patra, M.; Karttunen, M.; Hyvönen, M. T.; Vattulainen, I. Impact of Cholesterol on Voids in Phospholipids Membranes. *J. Chem. Phys.* **2004**, *121*, 12676−12689.
(41) Korlach, J.; Schwille, P.; Webb, W. W.; Feigenson, G. W. Characterization of Lipid Bilayer Phases by Confocal Microscopy and Fluorescence Correlation Spectroscopy. *Proc. Natl. Acad. Sci. U. S. A.* **1999**, *96*, 8461−8466.
(42) Flenner, E.; Das, J.; Rheinstädter, M. C.; Kosztin, I. Subdiffusion and Lateral Diffusion Coefficient of Lipid Atoms and Molecules in Phospholipid Bilayers. *Phys. Rev. E* **2009**, *79*, 011907.
(43) Luzar, A.; Chandler, D. Structure and Hydrogen Bond Dynamics of H2O-DMSO Mixtures by Computer Simulations. *J. Chem. Phys.* **1993**, *98*, 8160−8173.
(44) Borin, I. A.; Skaf, M. S. Molecular Association Between Water and DMSO in Solution: A MD Simulation Study. *J. Chem. Phys.* **1999**, *110*, 6412−6420.
(45) Elola, M. D.; Ladanyi, B. M. Computational Study of Structural and Dynamical Properties of Formamide-Water Mixtures. *J. Chem. Phys.* **2006**, *125*, 184506.
(46) Lopez, C. F.; Nielsen, S. O.; Klein, M. L.; Moore, P. B. Hydrogen Bonding Structure and Dynamics of Water at the Dimyristoylphosphatidylcholine Lipid Bilayer Surface from a Molecular Dynamics Simulation. *J. Phys. Chem. B* **2004**, *108*, 6603−6610.
(47) Alarcón, L. M.; de los Angeles Frías, M. d. A.; Morini, M. A.; Belen Sierra, M. B.; Appignanesi, G. A.; Anibal Disalvo, E. Water Populations in Restricted Environments of Lipid Membrane Interphases. *Eur. Phys. J. E: Soft Matter Biol. Phys.* **2016**, *39*, 94.
(48) Rapaport, D. C. Hydrogen Bonds in Water. Network Organization and Lifetimes. *Mol. Phys.* **1983**, *50*, 1151−1162.
(49) Martí, J.; Padró, J. A.; Guàrdia, E. Molecular Dynamics Simulation of Liquid Water along the Coexistence Curve: H-Bonds and Vibrational Spectra. *J. Chem. Phys.* **1996**, *105*, 639−649.
(50) Shell, S. M.; Debenedetti, P. G.; Panagiotopoulos, A. Z. Molecular Structural Order and Anomalies in Liquid Silica. *Phys. Rev. E: Stat. Phys., Plasmas, Fluids, Relat. Interdiscip. Top.* **2002**, *66*, 011202.
(51) Errington, J. R.; Debenedetti, P. G. Relationship Between Structural Order and the Anomalies of Liquid Water. *Nature (London, U. K.)* **2001**, *409*, 318−321.
(52) Errington, J. R.; Debenedetti, P. G.; Torquato, S. Quantification of Order in the Lennard-Jones System. *J. Chem. Phys.* **2003**, *118*, 2256−2263.
(53) Truskett, T. M.; Torquato, S.; Debenedetti, P. G. Towards a Quantification of Disorder in Materials: Distinguishing Equilibrium and Glassy Sphere Packings. *Phys. Rev. E: Stat. Phys., Plasmas, Fluids, Relat. Interdiscip. Top.* **2000**, *62*, 993−1001.
(54) Kumar, P.; Han, S. Dynamics of Two-Dimensional Monolayer Water Confined in Hydrophobic and Charged Environments. *J. Chem. Phys.* **2012**, *137*, 114510.
(55) Krott, L. B.; Bordin, J. R.; Barbosa, M. C. New Structural Anomaly Induced by Nanoconfinement. *J. Phys. Chem. B* **2015**, *119*, 291−300.
(56) Nettleton, R. E.; Green, M. S. Expression in Terms of Molecular Distribution Functions for the Entropy Density in a Infinite System. *J. Chem. Phys.* **1958**, *29*, 1365−1370.
(57) Errington, J. R.; Truskett, T. M.; Mittal, J. Excess-Entropy-Based Anomalies for a Waterlike Fluid. *J. Chem. Phys.* **2006**, *125*, 244502.
(58) Baranyai, A.; Evans, D. J. Direct Entropy Calculation from Computer Simulation of Liquids. *Phys. Rev. A: At., Mol., Opt. Phys.* **1989**, *40*, 3817−3822.
(59) Fogarty, A. C.; Laage, D. Water Dynamics in Protein Hydration Shells: The Molecular Origins of the Dynamical Perturbation. *J. Phys. Chem. B* **2014**, *118*, 7715−7729.
(60) Gnanasekaran, R.; Xu, Y.; Leitner, D. M. Dynamics of Water Clusters Confined in Proteins: A Molecular Dynamics Simulation Study of Interfacial Waters in a Dimeric Hemoglobin. *J. Phys. Chem. B* **2010**, *114*, 16989−16996.
(61) Rezus, Y. L. A.; Bakker, H. J. Observation of Immobilized Water Molecules around Hydrophobic Groups. *Phys. Rev. Lett.* **2007**, *99*, 148301.
(62) Titantah, J. T.; Karttunen, M. Long-Time Correlations and Hydrophobe-Modified Hydrogen-Bonding Dynamics in Hydrophobic Hydration. *J. Am. Chem. Soc.* **2012**, *134*, 9362−9368.

DOI: 10.1021/acs.jpcb.8b00360
J. Phys. Chem. B 2018, 122, 5897−5907